Mon. Not. R. astr. Soc. (1982) 199, 611–631

A complete sample of extragalactic radio sources at 1 Jy at 408 MHz – I. The radio observations

J. R. Allington-Smith *Mullard Radio Astronomy Observatory, Cavendish Laboratory, Madingley Road, Cambridge CB3 0HE*

Received 1981 September 4; in original form 1981 July 17

Summary. As part of the continuing investigation of the extragalactic radio source population, a complete sample of 59 B2 radio sources with flux densities between 1 and 2 Jy at 408 MHz has been studied. At this level the source counts exceed non-evolutionary predictions by the greatest amount, so a detailed analysis of the sample is expected to yield information about the sources responsible for this excess. In this paper the radio observations are described; these cover a wide range of angular scales from 1 arcsec to several arcmin, and a range of frequencies 0.4–5 GHz. The sample contains a wide variety of source types, including 'giant' sources of size > 1 Mpc, objects with extended structure of low brightness, sources showing spectral ageing, and compact objects. The median angular size is 12 arcsec.

A second paper in this series will present the results of a deep survey of the optical fields and all these data will be discussed in a third paper.

1 Introduction

The extragalactic radio source population evolves strongly, in the sense that the comoving number densities of powerful extragalactic radio sources increase dramatically with redshift (Longair 1966). In order to understand this phenomenon further, and to determine the dependence of source properties on cosmological epoch and on each other, a systematic study of 'complete' samples to different limits of flux density is required. This paper defines a new complete sample of moderate flux density (1–2 Jy at 408 MHz), representing the region where the observed counts of radio sources exceed non-evolutionary predictions by the greatest degree. Radio observations of this sample are presented, covering a wide range of angular scales and frequencies. The second paper in this series will present the results of a deep survey of the optical fields with a prototype CCD detector at the prime focus of the Hale 5-m telescope. Discussion and interpretation of these results, and a comparison with other work on samples in this flux density range (e.g. Swarup & Subrahmanya 1977; Grueff & Vigotti 1977; Katgert-Merkelijn, Lari & Padrielli 1980) will be presented in a third paper.

Several factors complicate the investigation of evolution of the radio source population. The total population may be made up of several sub-groups with different evolutionary properties. At least two such groups are known to exist, namely the 'steep-spectrum'

extended, and the 'flat-spectrum' compact, sources (Schmidt 1976; Wall, Pearson & Longair 1981; Peacock & Gull 1981). There may be other such groups, for instance 'giant' (> 1 Mpc) sources, and sources with very steep spectra of the type found in Abell clusters. It is necessary to identify each group so that it may be studied separately.

The dependence of source structures on radio luminosity in bright samples is well known (Fanaroff & Riley 1974; Jenkins & McEllin 1977; Neff & Rudnick 1980). The present sample contains a high proportion of actively evolving sources which may be preferentially of high luminosity (e.g. Longair 1966), so that comparison with other samples is not straightforward. There may also be a dependence of source structure on redshift, for example because of inverse Compton losses which could extinguish diffuse regions at high redshifts (Rees & Setti 1968; Rowan-Robinson 1970; Scheuer 1977).

In addition, the dependence of linear size on redshift or luminosity is unclear. It has been claimed that a dependence of linear size on redshift is required to explain both the observed small angular sizes of high-redshift sources (Miley 1971; Wills 1979) and the median angular sizes of flux-density-limited samples (e.g. Kapahi 1975, 1977), although an alternative possibility is that the linear size depends on radio luminosity (Stannard & Neal 1977; Hooley, Longair & Riley 1978; see also Downes, Longair & Perryman 1981 for further discussion). These conflicting findings may reflect biases in the data, in that the original samples are incomplete for sources of large angular size and that the subsequent determinations of radio structures miss extended regions of low brightness.

With these points in mind, three main objectives can be defined for these observations:

(1) The determination of radio structures, with particular attention to extended regions of low brightness. The 5-km telescope allows structure on scales down to 1 arcsec to be detected at 5 GHz, while extended structure can be detected by the one-mile telescope (OMT) at 0.4 and 1.4 GHz.

(2) The determination of radio spectra by covering wide ranges of frequency, using the available structural information to correct the flux densities for resolution and confusion effects. The spectra can yield structural information for sources whose structures are not determined from the brightness distributions alone (e.g. for cases in which synchrotron self-absorption or spectra ageing is seen). Such studies can also be useful in searching for correlations between spectral and other properties (e.g. the radio luminosity–spectral index correlation, Laing & Peacock 1980).

(3) The determination of expected positions for optical identifications.

2 The sample

2.1 SELECTION

The sample contains sources from the Bologna catalogue (Colla *et al.* 1970, 1972, 1973; Fanti *et al.* 1974) with $1 \leqslant S(408) < 2$ Jy, $b > 30°$, $34° \leqslant \mathrm{Dec} < 40°$, $\mathrm{RA} < 13^{\mathrm{h}}\,02^{\mathrm{m}}$. Excluding 1004 + 34B, listed by Grueff & Vigotti (1979) as part of 3C 236, there are 59 sources which satisfy these criteria.

2.2 COMPLETENESS

The Bologna catalogue quotes peak flux densities only, thus discriminating against sources large than the 3×10 arcmin^2 beam of the Northern Cross telescope. Thus a source of linear size 1 Mpc will have its flux density underestimated for $z < 0.03$–0.1 (depending on source orientation). Although such sources are expected to be rare (in the present sample, 1–4

sources are expected to have redshifts less than this), there is a possibility that the Bologna survey discriminates against nearby giant sources. However, the choice of a narrow flux-density rate means that this bias can be partially corrected, since some very extended sources with flux densities greater than the upper limit of the sample will be similarly affected and will therefore be included in the sample.

3 The observations and data reduction

3.1 THE OBSERVATIONS

Initially all sources were observed with the OMT (Ryle 1962) at 0.4 and 1.4 GHz and with the 5-km telescope (Ryle 1972) at 2.7 or 5.0 GHz. Following the reduction of the 5-km data, all sources apparently unresolved at 2.7 GHz were re-observed at 5 GHz, except for one source which was thought originally to have double structure. The main characteristics of the telescopes are listed in Table 1.

Table 1. Telescope characteristics.

Telescope	Frequency (GHz)	No. of spacings	HPBW in RA (× cosecδ in dec) (arcsec)	First grating radius (arcsec)	Stokes parameters received	Receiver noise (mJy/beam)	Flux density errors (see Section 3.2.2) (mJy)	(mJy)
5-km	5.0	16	2	40	$I-Q$	3	10	30
5-km	2.7	16	4	75	$I-Q$	2	10	30
One-mile	1.4	4	23	120	$I+Q$	2	20	50
One-mile	0.4	4	80	420	$I+Q$	5	60	100

3.2 DATA REDUCTION

The initial reduction procedure for the 5-km telescope data followed that described by Pooley & Henbest (1974). The visibility data were inspected for evidence of resolution or the presence of nearby sources. Unrelated objects whose grating responses obscured parts of the main source were removed by subtracting a point-source response from the map at that location. For apparently unresolved sources the 5-GHz map was remade with uniform grading to give higher resolution at the expense of increased sidelobe levels, and was then smoothed to a lower resolution to reveal any extended low-brightness structure and to enable the angular size to be estimated. In addition, flux density estimates obtained from the map and from the visibility data were compared to ensure that low-brightness structure or discrete sources had not been overlooked.

The general procedure with the OMT data followed that described by Elsmore, Kenderdine & Ryle (1966). Particular attention was given to sources which had earlier been found to be unresolved or whose structures were poorly determined at 5 GHz with the 5-km telescope. In an attempt to find low-brightness extended structure around these sources, compact components with grating responses that obscured the central region of the map were removed if they themselves were outside this area. The central region was then processed using the 'clean' algorithm of Högbom (1974) with the point-source response appropriate to each observation. The source parameters were determined as follows:

3.2.1 Positions for optical identifications

For unresolved or extended source without visible double structure, the position of the peak in the brightness distribution was measured from the visibility data or from large-scale

contour plots. For double sources without central components, the positions of the main peaks in the brightness distribution of each lobe were measured and the mean of these was taken as the target position for optical identifications (see Paper II for further discussion). For double sources with central components, the position was taken as that of the central component. The positional errors for an unresolved source are ~ 0.2 arcsec for both the 5- and 2.7-GHz observations (Ryle & Elsmore 1973).

3.2.2 Flux densities

For observations at 1.4, 2.7 and 5 GHz, flux densities were obtained from the visibility data and, for apparently unresolved sources, were compared with peak flux densities on the maps. At these frequencies, few bright sources are found within the field of view, so the errors are dominated by receiver noise, phase errors and the presence of faint sources.

At 408 MHz the field of view contains a large number of bright sources, so the visibility data are difficult to interpret. In these cases the flux densities have been determined from the maps alone. The errors are dominated by the presence of bright sources, since it is not possible to remove their grating responses completely because of random phase errors affecting the beamshape.

The flux densities were calibrated as described by Downes, Longair & Perryman (1981) and then converted to the scale of Baars *et al.* (1977). Two error classes have been defined for the observations and the values adopted are given in columns 8 and 9 of Table 1. Since the integrated polarizations of extragalactic radio sources rarely exceed a few per cent (e.g. Conway *et al.* 1972), these flux densities will be treated as total intensities. The effect of polarization on spectral properties will be discussed in Section 4.4.

3.2.3 Angular sizes

For double sources the angular size is taken to be the distance between the main peaks in the brightness distribution of each lobe. For sources which were apparently unresolved at 5 GHz, but for which the visibility data gave some evidence of resolution, the 5-GHz map was smoothed to a lower resolution (usually that of the 2.7-GHz observation) and the angular size was estimated by assuming two different model brightness distributions which are likely to be representative of the actual source structures.

The first model consists of two unresolved lobes with equal flux density, separated by a distance that defines the angular size. This distance can be estimated by measuring the ratio of the peak brightness of the smoothed map to that of the original map. The smallest significant distance is set by the noise on the two maps and is ~ 0.8 and ~ 1.3 arcsec for sources extended at PA 90° and 0° respectively. In the second model the brightness distribution consists of a bidimensional Gaussian. The angular size is taken as the larger of the two half-widths estimated from the apparent broadening of the point-source response on the two maps individually. The smallest significant value is set by random (mainly tropospheric) phase errors which continuously change the apparent position of the source and, over a full observation, broaden the point-source response by an amount of the order of the fractional phase error. Typical values for the 5-GHz observations correspond to a broadening of 10 per cent, which corresponds to smallest measurable values of ~ 0.9 and ~ 1.5 arcsec for the estimated angular size of a source extended at PA 90° and 0° respectively.

The largest of the values obtained by these methods was taken as the final estimate of the angular size. If the errors have been underestimated, the angular sizes will be correspondingly

overestimated but not significantly, since only sources which show clear evidence of resolution have been treated in this way. Some sources which had small angular sizes at 5 GHz were found to have extended structure at 0.4 or 1.4 GHz, and in these cases, angular sizes estimated from the structures seen at these frequencies (see Section 4.3) have been recorded in addition to the angular sizes found at 5 GHz.

4 Results

4.1 TABLE OF RESULTS

Table 2 summarizes the principal results and is arranged as follows:

(1) Name in Bologna catalogue.
(2) 4C name.
(3) and (4) RA and Dec of the expected position of the identification (see Section 3.2.1).
(5)–(8) Flux densities at 0.4, 1.4, 2.7 and 5.0 GHz respectively. The errors are given in column 8 of Table 1 for all measurements except those marked with asterisks, which have the larger errors listed in column 9 of Table 1.

Table 2. Source parameters.

(1)	(2)	(3)	(4)	(5)	(6)	(7)	(8)	(9)	(10)	(11)	(12)	(13)	(14)	(15)	(16)
Name		Position (1950.0)		Flux densities (Jy)				Spectral parameters					structure		Notes
B2	4C	RA	Dec	0.4	1.4	2.7	5 GHz	α_L	α_H	β	$\sigma(\beta)$	K	morph.	θ	refs.
0822+34A	34.28A	8 22 4.0	34 17 4	1.33	0.68	0.31		0.54	1.19	-1.57	0.27	0.27	I	18	V
0822+39	39.23B	8 22 5.51	39 29 33.7	1.54	1.16		0.37	0.23	0.91	-1.25	0.10		E(1)	1	
0823+37	38.25	8 23 49.6	37 58 31	1.28*	0.43	0.15		0.88	1.61	-1.78	0.48	0.05	I?	42	O,V
0824+35A	35.20	8 24 26.56	35 35 1.1	1.60	0.87	0.78	0.80	0.49	0.07	0.77	0.10		E(2)	2	O,V
0825+34		8 25 15.73	34 52 49.0	0.80	0.32	0.17	0.11	0.74	0.85	-0.19	0.30		E(3)	2	
0835+37		8 35 11.90	37 21 10.7	0.55	0.34		0.13	0.40	0.76	-0.68	0.31		E(1)	2	
0847+37	37.25	8 47 12.49	37 58 23.0	1.12	0.54	0.45		0.60	0.25	0.84	0.28	0.12	II?C	33	
0854+39		8 54 29.3	39 57 12	1.28*	0.54	0.29		0.70	0.92	-0.54	0.35	0.33	II	164	
0857+39		8 57 41.7	39 7 59	1.17	0.56	0.33		0.60	0.78	-0.44	0.30	0.58	II	24	
0902+34		9 2 24.77	34 19 57.8	0.85*	0.34		0.13	0.74	0.76	-0.04	0.32		E(3)	10/1	
0908+37		9 8 45.3	37 36 33	1.41	0.57	0.42		0.73	0.44	0.72	0.27	0.16	II	33	GG
0913+39	38.28	9 13 39.54	39 7 1.9	1.41	1.07	0.78	0.66	0.22	0.39	-0.31	0.10		E(1)	2	
0922+36B	36.14	9 22 34.18	36 40 4.4	1.52*	0.73	0.48		0.59	0.66	-0.16	0.25	0.09	IC	100	H,GG,C,SA,V
0927+35		9 27 52.78	35 16 51.1	0.87	0.50		0.36	0.44	0.27	0.32	0.19		E(2)	50/3	
0952+35	35.21	9 52 48.9	35 47 38	1.50	0.55	0.24		0.82	1.24	-1.03	0.32	0.90	II	18	C,SC,V,PO
0955+38A	38.30	9 55 1.7	38 44 20	1.28	0.39	0.23		0.96	0.80	0.39	0.40	0.83	II*	19	O,V
1011+36		10 11 17.23	36 32 33.7	0.69	0.33		0.10*	0.60	0.95	-0.63	0.32		E(3)	40	
1016+36		10 16 58.50	36 37 51.5	1.19	0.55	0.33	0.25	0.63	0.62	0.02	0.17		E(3)	100/1	
1017+37	37.27A	10 17 44.7	37 12 8	1.01	0.45		0.13	0.65	0.99	-0.63	0.23	0.68	II	7	
1018+37	37.27B	10 18 19.2	37 29 34	0.65	0.31*		0.07	0.60	1.18	-1.06	0.58	0.09	II	61	V
1019+39B	39.31	10 19 58.8	39 24 0	1.28*	0.45		0.13	0.84	0.99	-0.28	0.25	0.85	II	7	O,V
1025+39	39.32	10 25 49.33	38 59 57.7	1.34	0.64	0.49	0.39	0.60	0.39	0.38	0.14		E(2)	2	
1035+36	36.17	10 36 0.7	36 16 55	0.91	0.30	0.17		0.90	0.85	0.12	0.53	0.91	II*	8	
1042+39	39.33	10 42 23.6	39 12 25	1.42	0.68		0.21	0.59	0.93	-0.62	0.15	0.81	II	9	O
1043+37A	37.28	10 43 21.87	37 14 32.0	0.98	0.26	0.11	0.07	1.08	1.03	0.09	0.38		E(3)	3	O,V
1049+38		10 49 22.35	38 27 40.6	1.17	0.67	0.39	0.25	0.45	0.78	-0.60	0.16		U(1)	<1	
1056+39		10 56 23.1	39 41 6	0.85*	0.33	0.16		0.77	1.09	-0.79	0.57	0.91	II?	15	
1100+35		11 0 40.9	35 5 57	0.98	0.31	0.20*	0.11	0.93	0.82	0.21	0.52	0.35	I/II	12	
1101+38		11 1 40.58	38 28 42.8	0.98	0.63	0.55	0.74	0.36	-0.13	0.91	0.15		E(2)	240/1	KP,U,WJ
1104+36	36.18	11 4 41.6	36 32 25	1.63	0.64	0.41		0.76	0.66	0.23	0.24	0.47	II	20	O
1106+37		11 6 43.43	38 0 47.3	1.09	0.92	0.91	0.70	0.14	0.22	-0.15	0.12		E(1)	1	
1108+39		11 8 33.57	39 56 31.9	0.80	0.38	0.23		0.60	0.76	-0.38	0.43	0.42	IIC	14	
1113+34	34.34	11 13 47.7	34 58 47	1.09	0.43	0.25		0.74	0.82	-0.19	0.37	0.72	II*	14	
1125+37	37.30	11 25 49.8	37 45 27	0.69*	0.40	0.17	0.11	0.44	1.03	-1.08	0.35	0.44	IIC?	7	O,V
1129+35		11 29 53.9	35 9 52	0.75*	0.42	0.29		0.46	0.56	-0.24	0.47	0.79	II*	13	
1129+37	37.31	11 29 55.5	37 10 51	1.06	0.49	0.22		0.62	1.22	-1.47	0.37	0.86	II*	14	O,V
1130+34	34.35	11 30 6.3	34 56 12	1.63	0.52*	0.38		0.92	0.48	1.06	0.52	0.29	II	78	
1132+37		11 32 26.37	37 25 16.1	1.40	0.65		0.26	0.62	0.73	-0.20	0.15		E(3)	1	
1141+35	35.26	11 41 13.7	35 25 0	0.85*	0.29		0.11	0.88	0.76	0.20	0.36	0.59	II	10	
1143+37		11 43 1.23	37 3 7.4	1.17*	0.44		0.14	0.79	0.91	-0.23	0.26		U(3)	<1	
1148+36A	36.19	11 48 13.8	36 38 43	1.71	0.67	0.24		0.76	1.56	-1.94	0.29	0.13	II?	27	H,O,SA,V
1148+38	38.31	11 48 53.33	38 42 33.5	1.70	0.64	0.36	0.24	0.79	0.78	0.03	0.14	0.64	II?C	9	O,V
1159+36		11 59 20.92	36 51 36.0	0.94	0.34	0.21	0.11	0.82	0.89	-0.14	0.28		E(3)	2	
1201+39		12 1 33.78	39 28 59.7	0.91	0.55	0.23	0.17	0.41	0.92	-0.95	0.20		E(1)	3	
1204+37	37.33	12 4 22.1	37 8 18	1.96	0.65	0.31		0.89	1.12	-0.54	0.26	0.55	II	51	O,V
1204+35	35.27	12 4 59.4	35 19 45	1.50	0.48	0.28		0.92	0.82	0.23	0.33	0.75	II*	16	O,V
1204+34		12 5 0.38	34 9 21.6	1.13	0.46	0.20		0.72	1.27	-1.34	0.39	0.38	IIC	48	GG
1207+38		12 7 37.7	38 37 56	0.89	0.35	0.17		0.76	1.09	-0.81	0.49	0.71	II	27	
1212+38A		12 12 26.06	38 5 31.1	0.98	0.28	0.15	0.07	1.02	1.09	-0.14	0.37		U(3)	<1	
1217+36	36.20	12 17 40.13	36 45 45.5	1.12	0.38	0.21		0.87	0.90	-0.06	0.42		U(3)	<2	
1220+37		12 20 42.28	37 23 38.4	1.11	0.50	0.27		0.64	0.94	-0.75	0.34	0.47	IIC	36	
1225+36		12 25 30.78	36 51 46.9	0.99	2.18		0.87	-0.64	0.72	-2.50	0.11		U(1)	<1	F,KS
1230+34	34.37	12 30 13.9	34 59 21	1.40	0.47	0.27		0.87	0.84	0.07	0.34	0.85	II?	11	
1245+34		12 45 23.4	34 21 34	0.93	0.44	0.25	0.17	0.60	0.76	-0.30	0.22	0.56	II?	6	K1,K2
1255+37	36.22	12 55 2.26	37 0 31.1	1.51	0.64	0.47	0.33	0.70	0.53	0.32	0.14		E(2)	1	GK,K1,K2,O,V
1256+36		12 56 44.8	36 48 9	1.31*	0.51	0.33		0.75	0.66	0.22	0.34	0.70	II*	15	K1,K2
1257+34		12 57 31.70	34 13 2.6	1.06	0.47	0.30	0.19	0.66	0.73	-0.13	0.20		U(3)	<1	K2
1301+38A	38.35	13 1 24.3	38 12 13	1.54	0.67	0.27		0.68	1.37	-1.70	0.28	0.41	II	28	H,K1,K2,SA,V
1301+35		13 1 32.76	35 25 55.7	0.87	0.39	0.32	0.26	0.65	0.33	0.59	0.22		U(2)	<1	K1,K2,O

(9) Low-frequency spectral index α_L between 0.4 and 1.4 GHz. (In this paper spectral index is always defined in the sense $S \propto \nu^{-\alpha}$.)

(10 High-frequency spectral index α_H between 1.4 and 5 GHz, or between 1.4 and 2.7 GHz when the source has not been observed at 5 GHz.

(11) Spectral curvature index β defined as $2(\alpha_L - \alpha_H)/\log_{10}(F/0.408\,\text{GHz})$ where F is either 2.7 or 5.0 GHz depending on the definition of α_H.

(12) The estimated uncertainty in the spectral curvature index $\sigma(\beta)$.

(13) Value of the parameter K for the double sources, defined as the ratio of the sum of the peak flux densities in the lobes to the total flux density for the highest frequency observation. This parameter must be interpreted with caution since it measures the flux density within one beamwidth of the peaks in brightness of each lobe, and the linear size of the beam is a function of redshift (and the telescope resolution); thus an apparent correlation of this parameter with redshift (or radio luminosity) will always be found.

(14) Morphology. The classification scheme of Fanaroff & Riley (FR) is used. The measured parameter is the ratio of the distance between the peaks in the brightness distribution of each lobe to the distance between the outermost contours on opposite sides of the source. If this ratio is < 0.5 the source is assigned to class I, if the ratio is > 0.5 the source is assigned to class II (an asterisk indicates that the lobes are unresolved). Sources of intermediate class are indicated at 'I/II'. Unresolved sources (i.e. with angular sizes less than 1 arcsec) are indicated by 'U', while extended sources lacking visible structure are indicated by 'E' (the figures in parentheses refer to Section 4.5). Central components are indicated by 'C'.

(15) Angular size θ in arcsec. If different angular sizes have been estimated from the low- and high-resolution observations then both are given, separated by a solidus.

(16) References to other work. 5-GHz flux densities obtained from the 100-m Effelsberg telescope and optical identifications on the Palomar Observatory–National Geographic Society Sky Survey plates (based on positional coincidence within 15 arcsec) for all sources are given by Grueff & Vignotti (1979). The references are abbreviated as follows: F – Folsom *et al.* (1971), GG – Gioia & Gregorini (1980), GK – Galt & Kennedy (1968), H – Hine (1981; see also Wilkinson, Hine & Sargent 1981), K1 – Katgert (1976), K2 – Katgert *et al.* (1973), KP – Kapahi (1979), KS – Kraus & Scheer (1967), O – Olsen (1967, 1970), PW – Peacock & Wall (1981), SA – Sargent (1973), SC – Schmidt (1974), U – Ulrich *et al.* (1975), V – Véron & Véron (1979), and WJ – Weiler & Johnston (1980).

4.2 CONTOUR PLOTS

Fig. 1 shows contour plots of the sources which have significant structure.

4.3 NOTES ON INDIVIDUAL SOURCES

Only the radio properties are discussed here, except in a few cases, either where knowledge of the optical identification from Paper II is necessary to understand the source structure or where there are features of particular interest.

0823 + 37. Very diffuse structure without clearly defined hotspots. The spectrum is very steep at high frequency. The curvature of the spectrum and the lack of hotspots suggest that the emitting regions are not being replenished with electrons. 1148 + 36A is similar.

0847 + 37. Faint double structure with a very bright central component producing half the total flux density at 2.7 GHz.

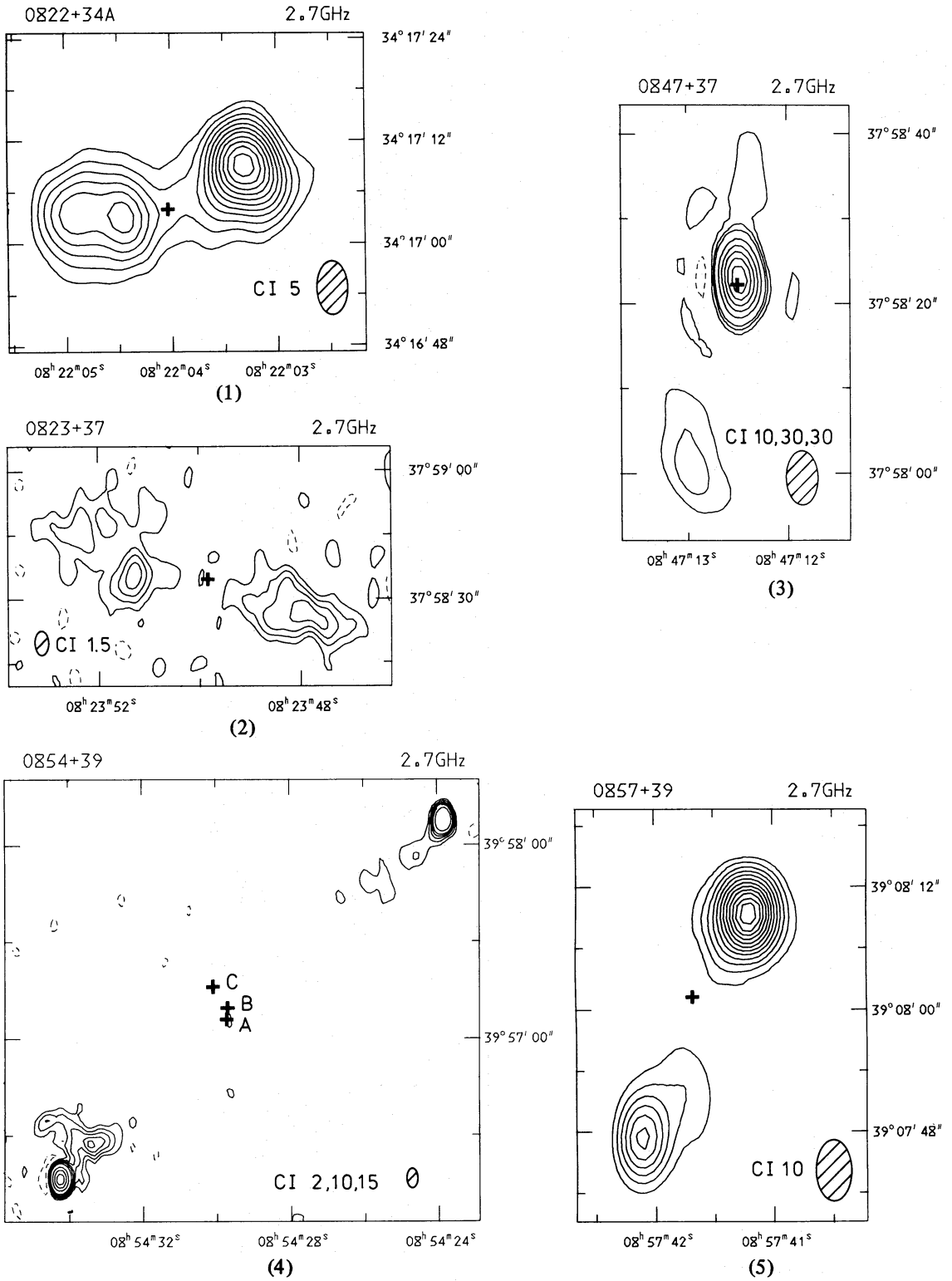

Figure 1. Contour plots for those sources which have significant structure. The half-power synthesized beamwidth is represented by a shaded ellipse. The contour interval in mJy/beam is indicated beside the letters 'CI'. In some cases, two contour intervals are used, in which case the three numbers refer to the initial contour interval, the maximum contour for that interval and the subsequent interval respectively. All zero contours are omitted, negative contours are shown broken and are always drawn at the initial contour interval. Crosses mark the positions of optical objects which are discussed in Paper II. For the source 1018 + 37, contour plots are shown for both the 1.4- and 5-GHz observations, since neither fully represents the source structure.

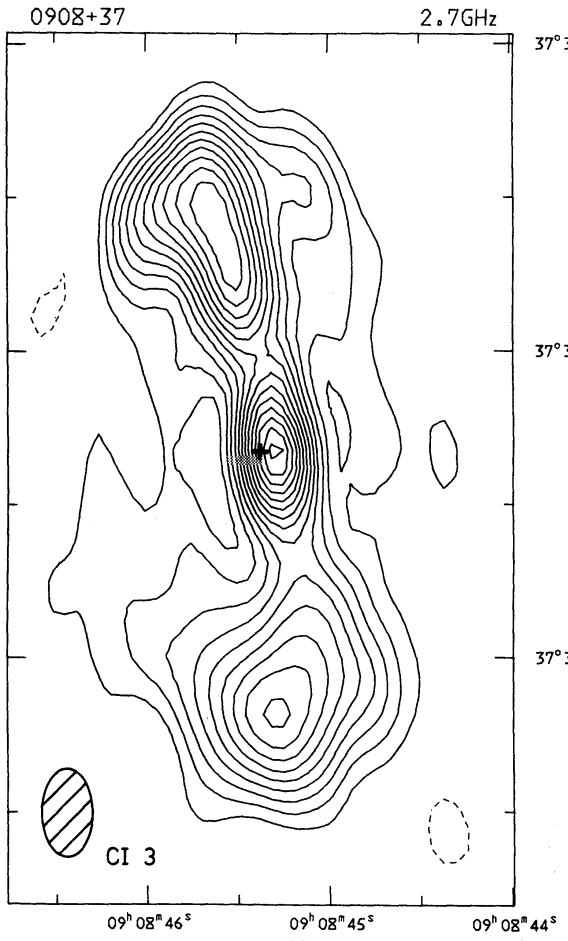

(6)

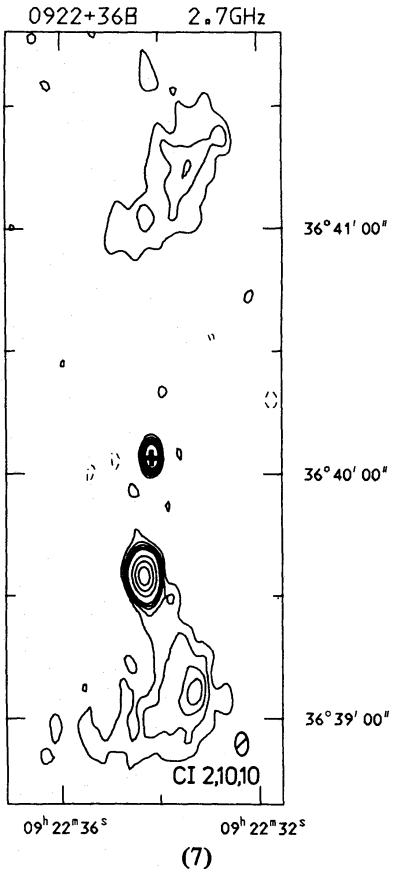

(7)

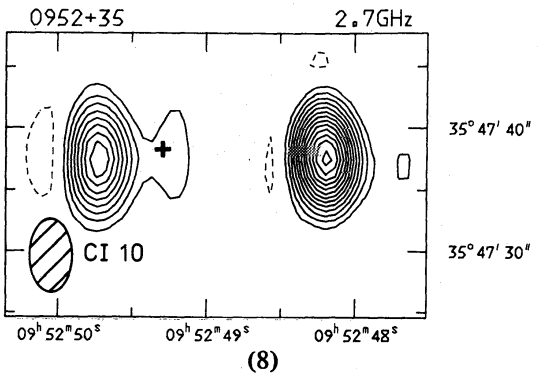

(8)

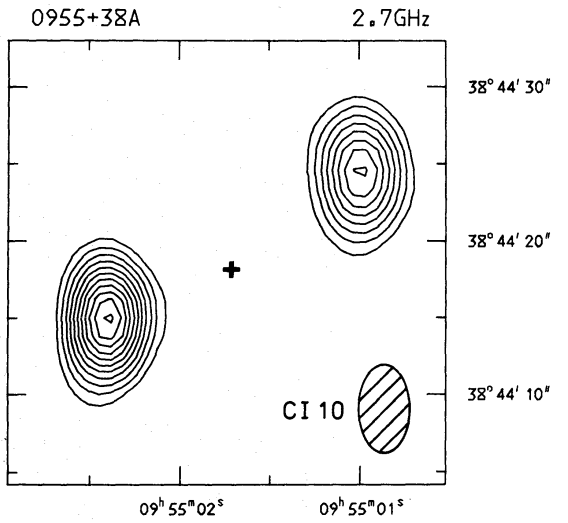

(9)

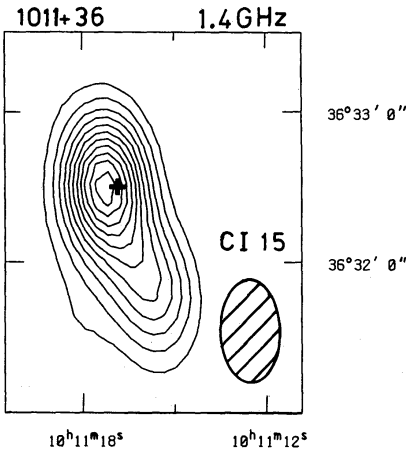

(10)

Figure 1. – *continued*

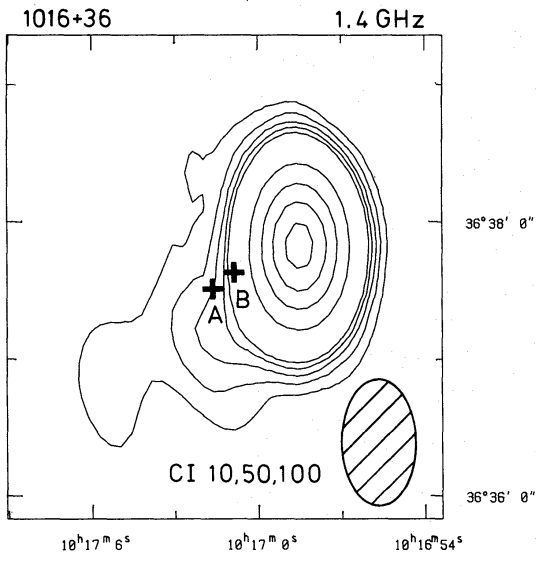

(11)

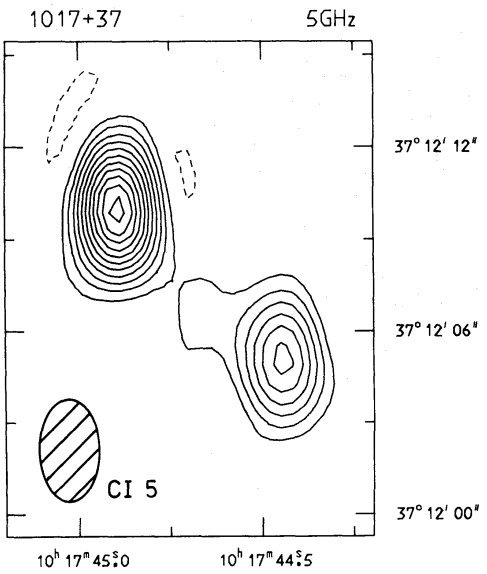

(12)

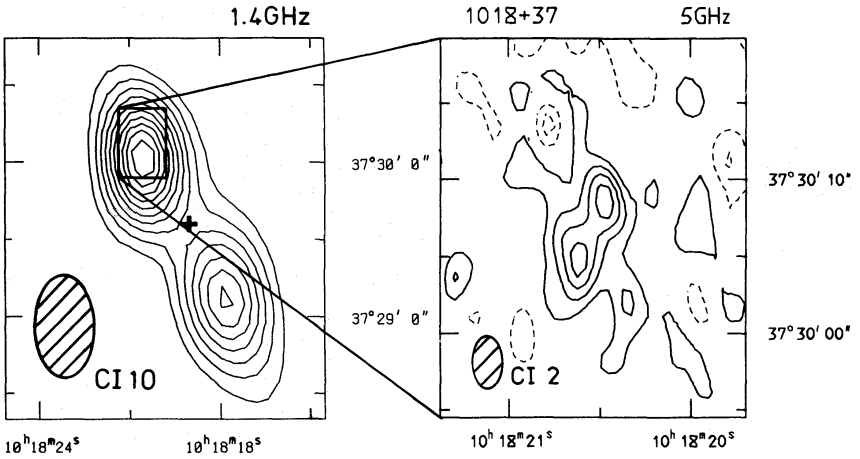

(13)

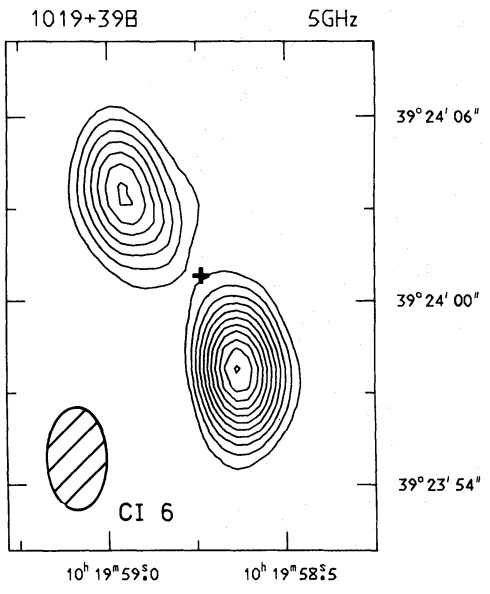

(14)

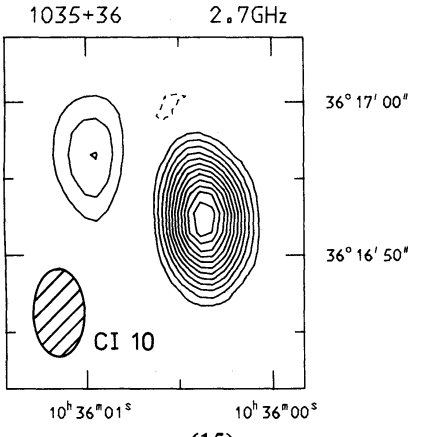

(15)

Figure 1. – *continued*

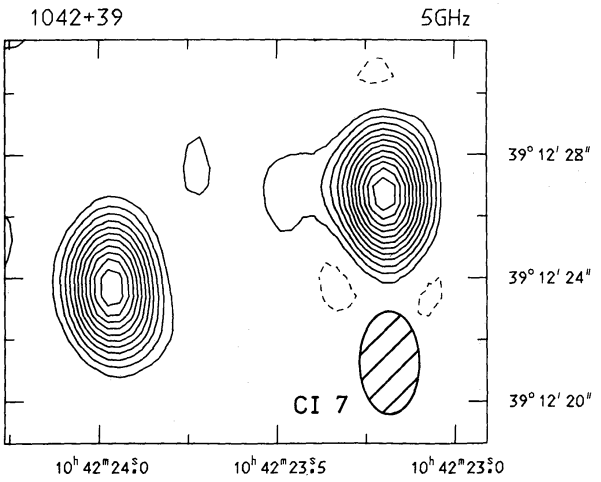

(16)

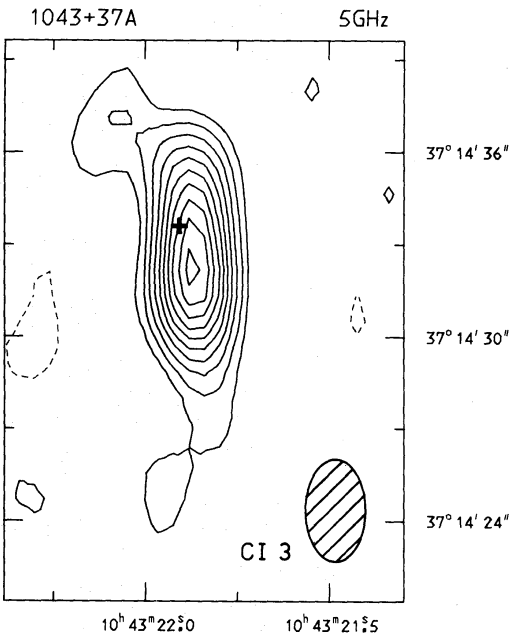

(17)

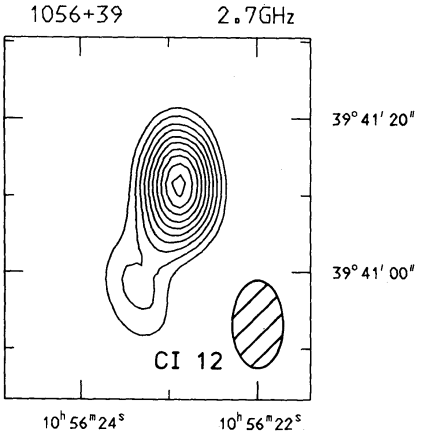

(18)

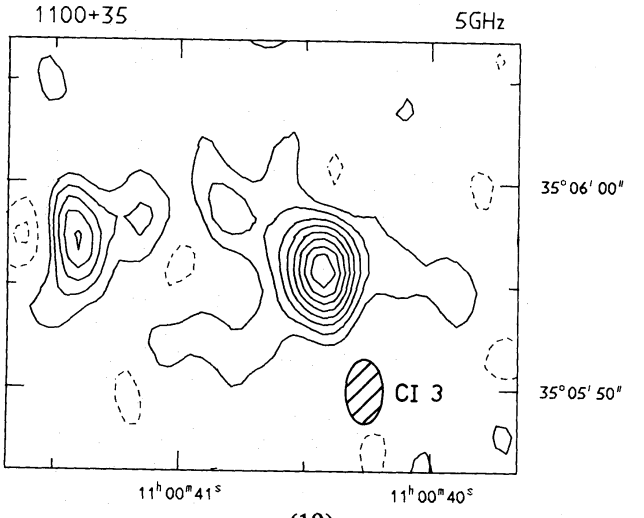

(19)

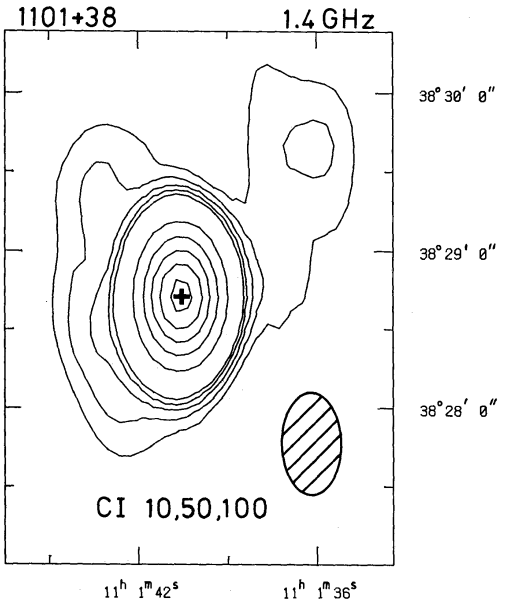

(20)

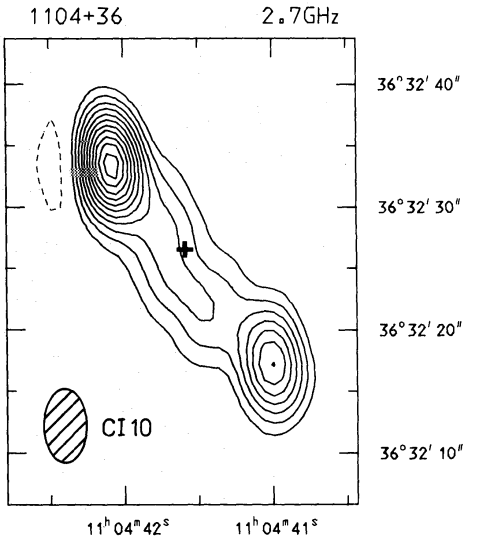

(21)

Figure 1. – *continued*

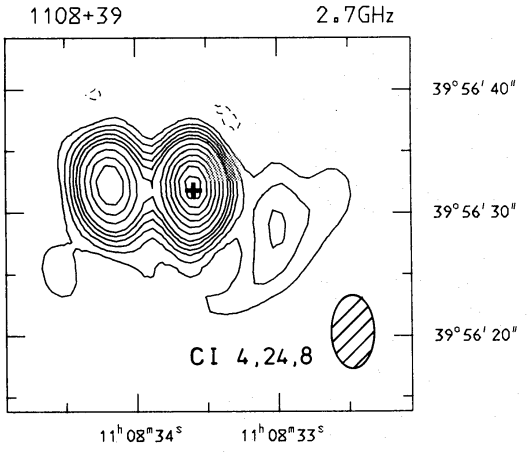

(22)

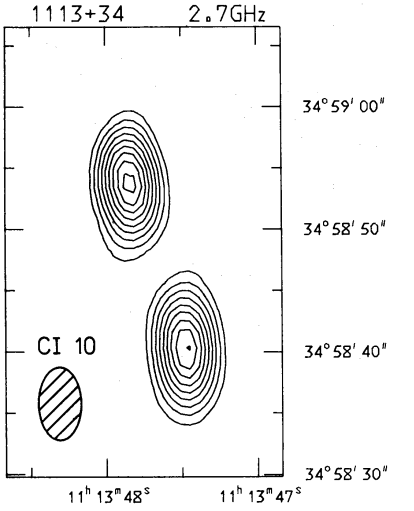

(23)

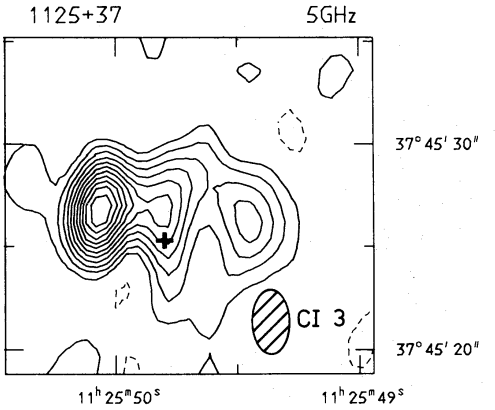

(24)

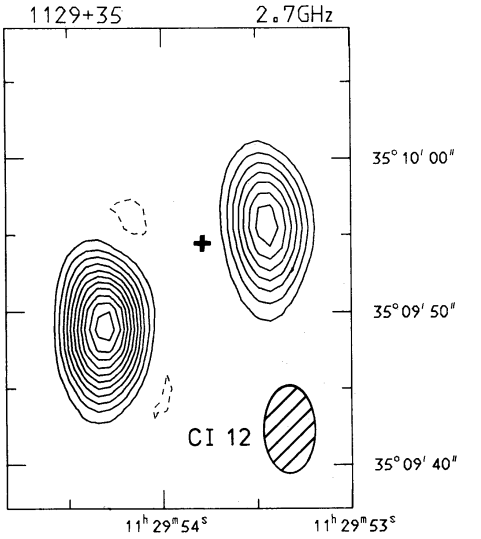

(25)

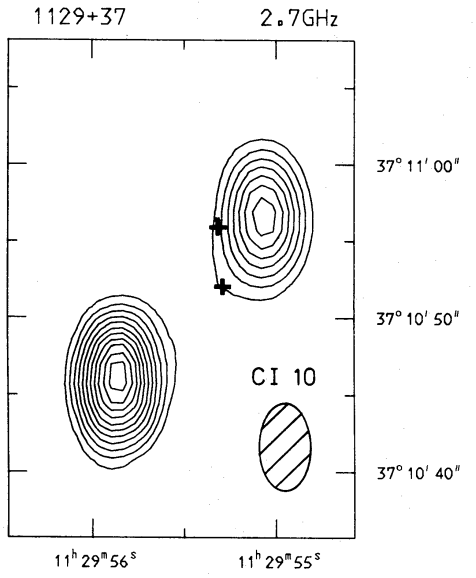

(26)

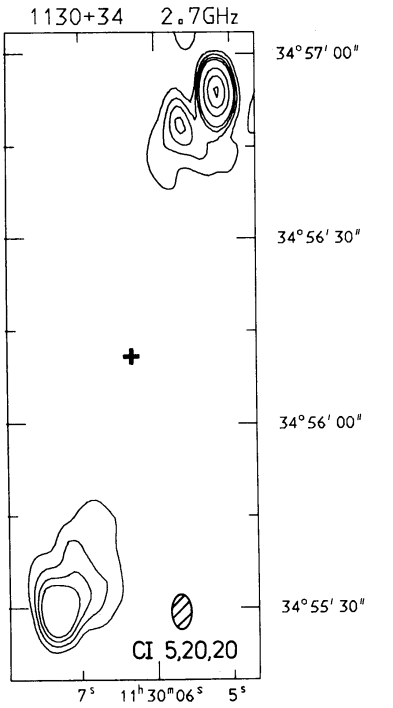

(27)

Figure 1. – *continued*

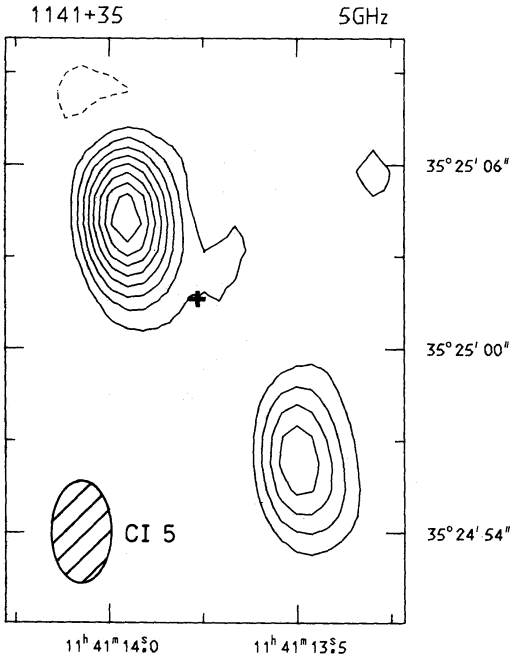

(28)

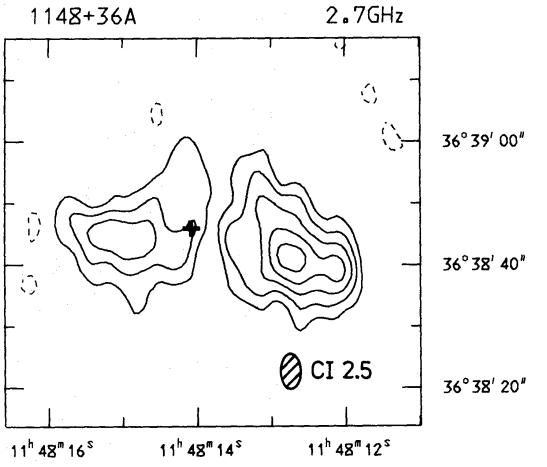

(29)

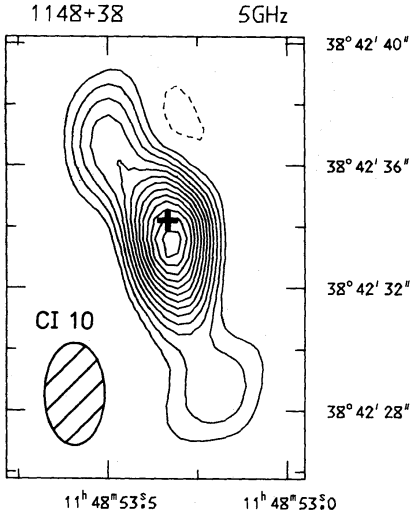

(30)

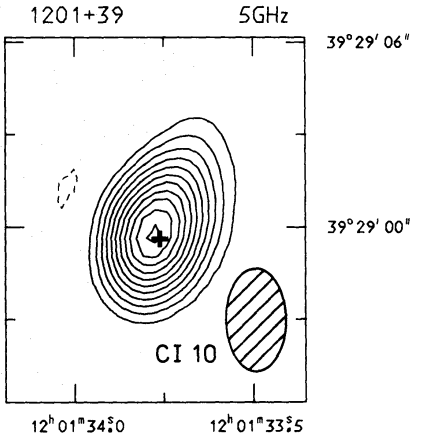

(31)

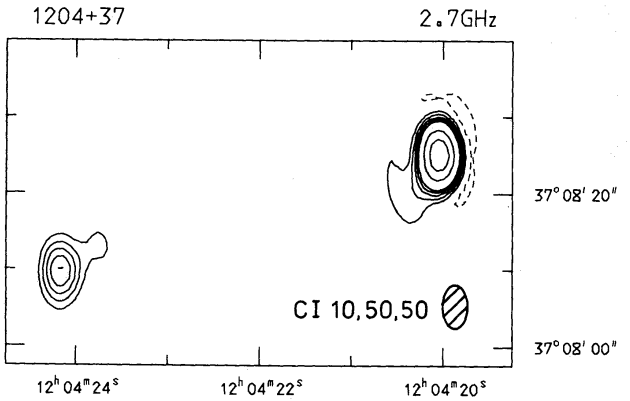

(32)

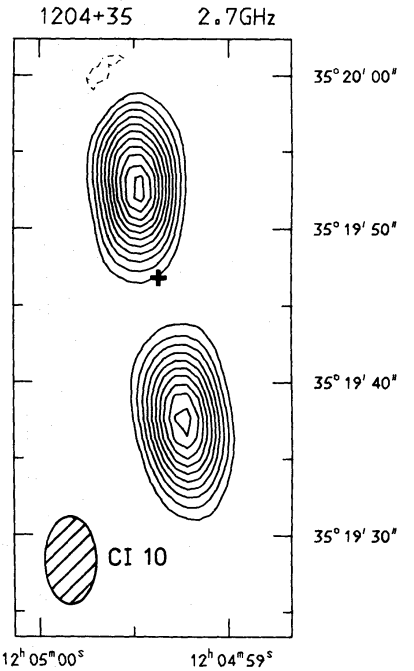

(33)

Figure 1. – *continued*

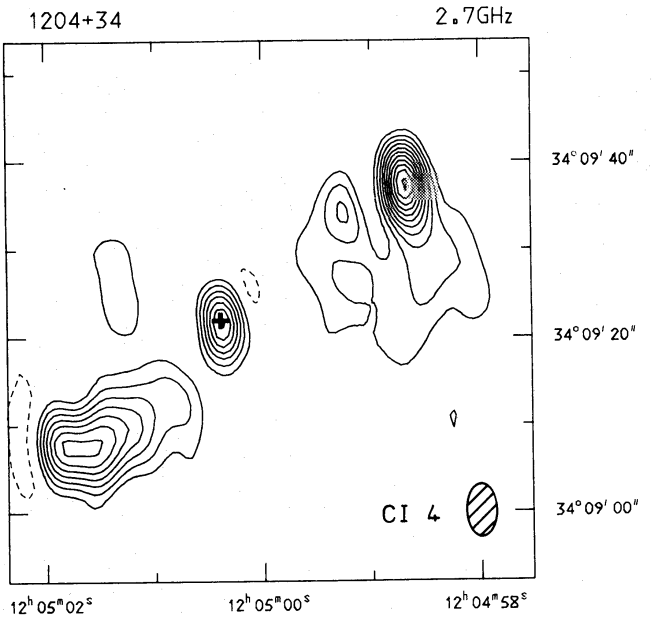

(34)

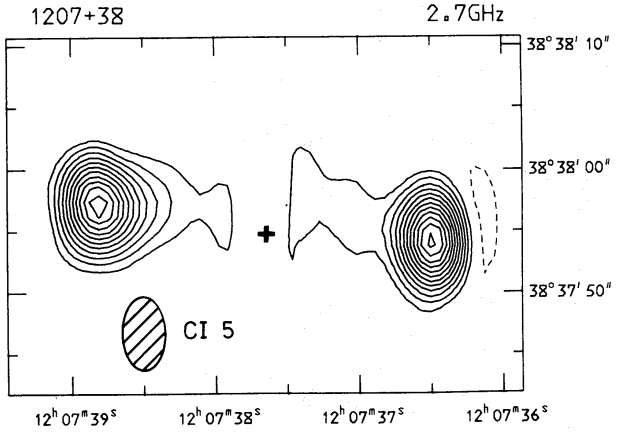

(35)

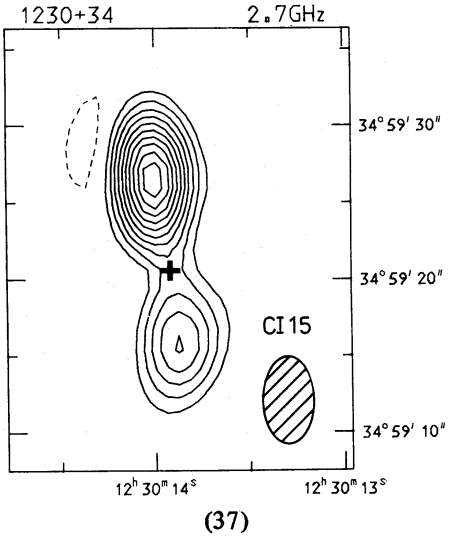

(37)

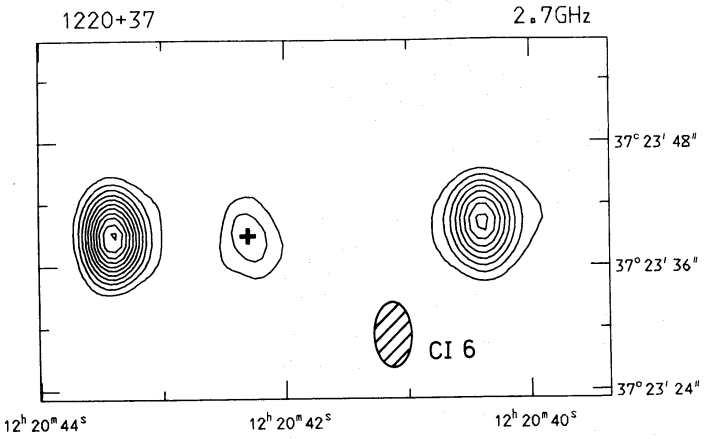

(36)

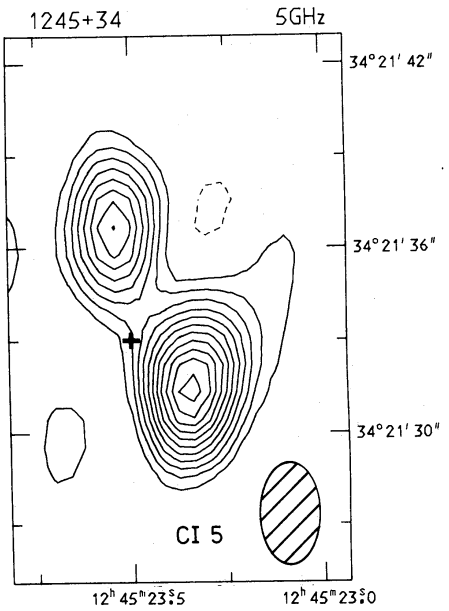

(38)

Figure 1. – *continued*

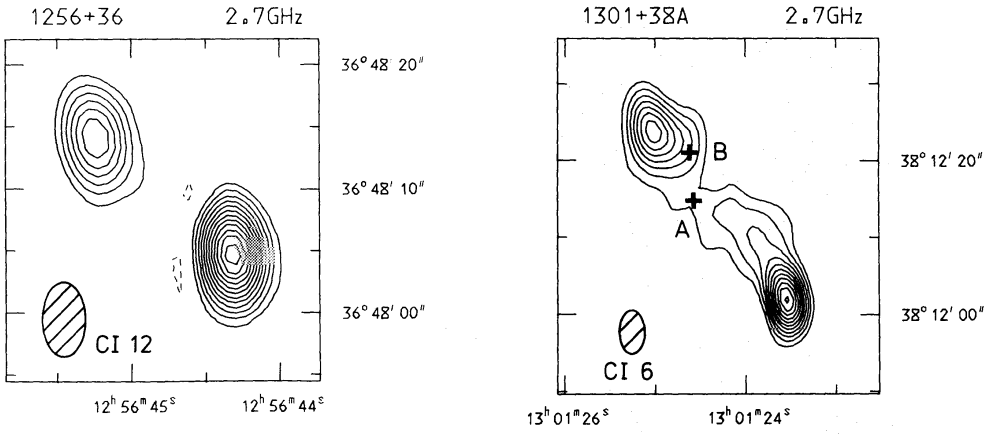

(39) (40)

Figure 1. – *continued*

0854 + 39. From the apparent magnitude of the optical identification it is likely that the projected linear size of this source is > 1 Mpc.

0902 + 34. At 5 GHz the source is slightly resolved in a N–S direction. At 1.4 GHz there is evidence from the visibility data that the source is resolved at PA 100°–130°. At 0.4 GHz the map shows a possible extension at PA ~ 90° as well as a faint extended region 4 arcmin away at PA 120° which is not seen at 1.4 GHz (there is also slight evidence for an extended region 5 arcmin away at PA ~ 180°). The spectrum is steep and straight, and the source is optically unidentified.

0908 + 37. Extended structure without clearly defined hotspots. A central component is present but is well resolved along the source axis. (Paper II shows that the radio source is still confined within the environs of the optical galaxy.)

0922 + 36B. Only the southern lobe of this source has a hotspot. This lobe shows diffuse structure with a secondary peak in brightness further to the south. The source has been labelled as FR class I, since the southern lobe is clearly of this type and the extent of the northern lobe is poorly determined.

0927 + 35. At 5 GHz the source is resolved at PA ~ 20°. At 1.4 GHz there is evidence of an extension at PA ~ 90°. No structure is seen at 0.4 GHz, implying that all the structure has been detected at 1.4 GHz. The angular size, estimated from the 1.4-GHz map, is ~ 50 arcsec. The spectrum is flat and the source is optically identified.

1011 + 36. At 5 GHz an unresolved feature with half the total flux density is seen, with a very low-brightness extension to one side at PA ~ 210°. At 1.4 GHz the extension is ~ 1 arcmin along at the same position angle, with further extended emission surrounding the source. No extended emission is seen at 0.4 GHz, implying that all the structure has been detected at 1.4 GHz. The unresolved feature is optically identified. A faint unresolved source with an inverted spectrum lies 4 arcmin away at PA 190°.

1016 + 36. At 2.7 and 5 GHz the source appears to be slightly resolved in a N–S direction. At 1.4 GHz a low-brightness extension nearly 2 arcmin long is seen at PA 120°. No extended structure is seen at 0.4 GHz, implying that all the structure has been detected at 1.4 GHz. The source has a faint optical identification, implying that the linear size may be ~ 1 Mpc. There is possibly a further extended region of emission 2 arcmin away at PA 160°.

1018 + 37. At 5 GHz only a faint double structure is detected which, at 1.4 GHz, is seen to be a pair of hotspots in the northern lobe of an extended double source. The angular size is measured from the 1.4-GHz map. The spectrum shows pronounced high-frequency steepening.

1025 + 39. There are two nearby faint sources 1.5 and 3 arcmin away at PA 290° and 320° respectively. The source is optically identified.

1043 + 37A. This source is extended in a N–S direction with brightness falling off from the centre. Lower resolution maps show no further structure. The source is optically identified.

1101 + 38. At 2.7 GHz the source is slightly resolved at PA ~ 30°, whereas at 5 GHz it is unresolved. At 1.4 GHz, low-brightness regions are detected on either side of the source with a total extent of ~ 4 arcmin. At 0.4 GHz the source is slightly extended at approximately the same PA, but no further extended structure is seen. This implies that the angular size cannot greatly exceed 4 arcmin, and this is the final value adopted. The spectrum is flat between 0.4 and 1.4 GHz and curves upwards at higher frequency. The optical identification is a BL Lac object (Markarian 421).

1106 + 37. Misidentified in the Bologna catalogue with 4C 37.29A.

1108 + 39. The optical identification coincides with the main peak in brightness, indicating that this is a central component.

1148 + 36A. This source is very similar to 0823 + 37 in spectrum and structure, and the same deductions can be made about its nature.

1217 + 36. A faint steep-spectrum source lies 40 arcsec away at PA 80°. Both sources are optically identified, indicating that they are probably unrelated.

1255 + 37. There are faint sources 1 and 3 arcmin away at PA 60° and 290° respectively. The source is optically identified.

1301 + 35. Possibly extended in a N–S direction at 0.4 and 1.4 GHz.

4.4 SPECTRAL PARAMETERS

There are at least three flux-density measurements for each source and so three spectral parameters have been defined: the low- and high-frequency spectral indices (α_L and α_H) and the spectral curvature index β (Section 4.1). As $\beta = -\Delta\alpha/\Delta \log_{10}(\text{frequency})$, high-frequency steepening is indicated by $\beta < 0$. Although the use of two alternative frequencies in the definition of α_H is undesirable and could lead to a bi-modal distribution if the spectra are highly curved between 2.7 and 5.0 GHz, the mean value of α_H should nevertheless be an indicator of spectral shape. The distribution of β should not suffer from this problem provided that the spectral curvature is approximately constant. Individual values of α_H and β will be affected by the integrated polarization of the source, since $I - Q$ has been measured at 2.7 and 5 GHz and $I + Q$ at 0.4 and 1.4 GHz. Taking typical values of polarization found in the literature (e.g. Conway *et al.* 1972 and references therein) for samples of sources resembling those in the 3C catalogue, it is expected that, for the present sample (in the absence of evidence that polarization depends on flux density), α_H will be changed by ~ 0.05 and β will be changed by ~ 0.1, however the mean values will be unaffected.

The distributions of these three parameters are given in Figs 2–4 for (a) all sources, (b) sources with $\theta > 1$ arcsec and (c) sources with $\theta \leqslant 1$ arcsec.

4.4.1 Low-frequency spectral index distribution (Fig. 2)

The overall distribution shows an approximately Gaussian shape with a small tail extending towards low values. The mean is 0.65 and the standard deviation 0.26. Twelve sources have $\alpha_L < 0.5$. The $\theta > 1$ arcsec distribution is more symmetrical, with a higher mean (0.69) and a smaller dispersion (0.18). Eight sources with $\theta > 1$ arcsec have $\alpha_L < 0.5$. The $\theta \leqslant 1$ arcsec distribution has a lower mean (0.46) and a higher standard deviation (0.44), reflecting the higher proportion of flat-spectrum sources in this range of angular size.

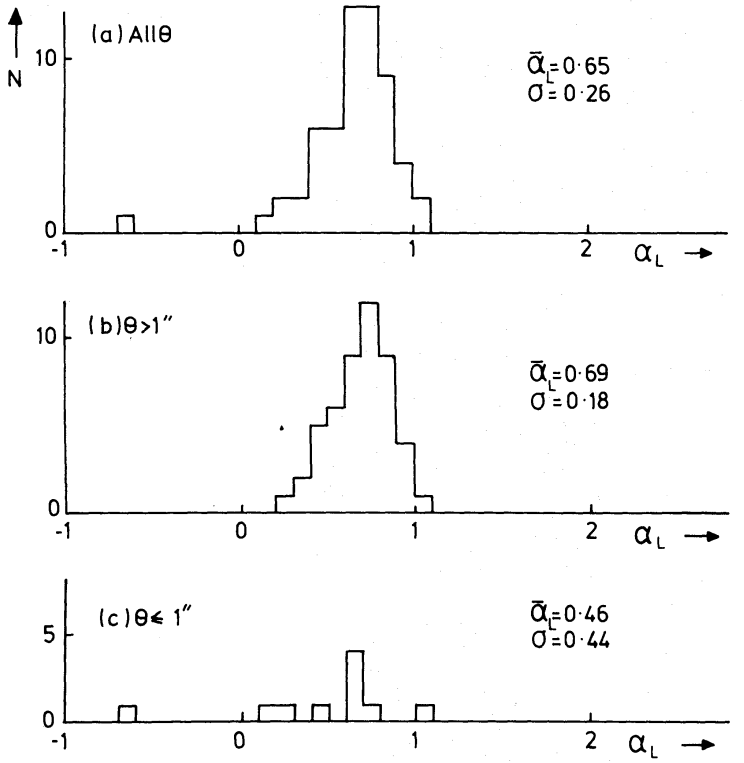

Figure 2. Distribution of low-frequency spectral index α_L. For this figure and Figs 3 and 4 the distributions are plotted separately for (a) all sources, (b) sources with $\theta > 1$ arcsec, (c) sources with $\theta \leqslant 1$ arcsec. Means and standard deviations for each distribution are indicated by the appropriate symbol with a bar and σ respectively.

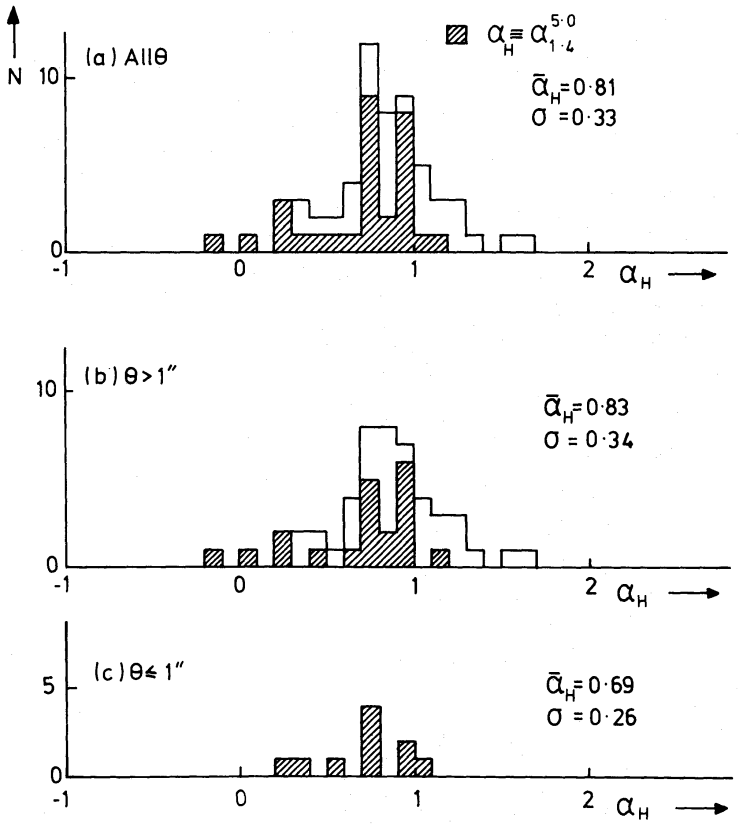

Figure 3. Distribution of high-frequency spectral index α_H. Values derived from 5-GHz observations are shown shaded.

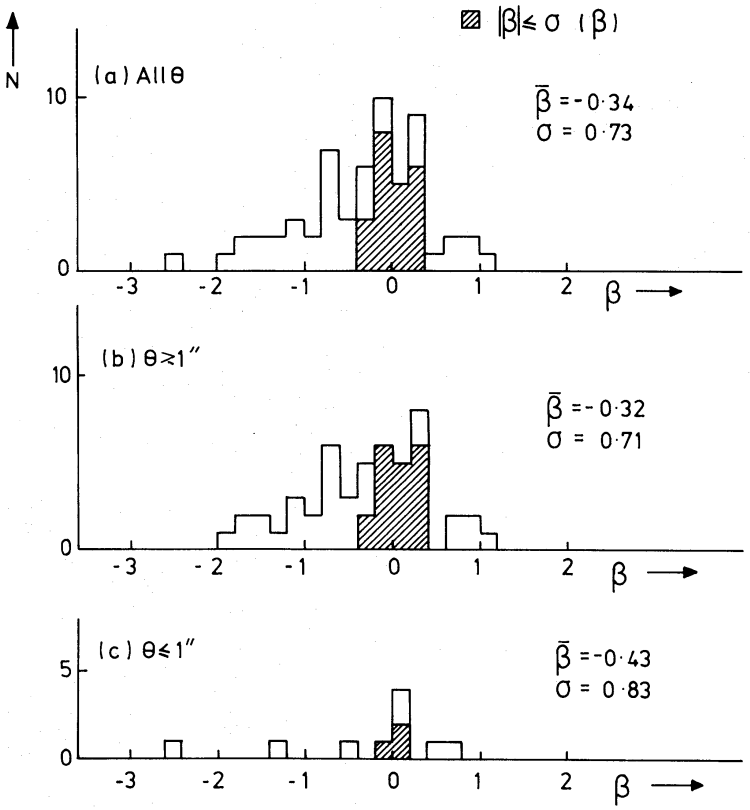

Figure 4. Distribution of the spectral curvature index β, defined in Section 4.1. Values which indicate straight spectra are shown shaded.

4.4.2 High-frequency spectral index distribution (Fig. 3)

In these distributions the values obtained from 5-GHz measurements are shown shaded. With a dispersion of 0.33 this distribution is much broader than that for α_L and the mean value of 0.81 is significantly higher, indicating that the spectra tend to steepen at high frequencies. The broadening of the distribution is probably not caused by the use of two alternative frequencies in the definition of α_H, since the highest values are not preferentially derived from the 5-GHz measurements (as would otherwise be expected since the overall trend is for negative curvature). There are 10 sources with $\alpha_H < 0.5$. The distribution for $\theta > 1$ arcsec retains the dispersion of the parent distribution but with a higher mean (0.83), implying that the broadening is caused mostly by the extended steep-spectrum sources which also show the most spectral steepening. The $\theta \leqslant 1$ arcsec distribution has a mean value of 0.69 and a standard deviation of 0.26. The mean is higher than for the $\theta < 1$ arcsec sources in the α_L distribution, as one would expect if some of these sources are of the steep-spectrum type and show high-frequency steepening like the sources with $\theta > 1$ arcsec.

4.4.3 Curvature index distribution (Fig. 4)

In these distributions the hatched boxes represent sources with spectra that are, within the errors, straight. The overall distribution has a broad asymmetric shape (standard deviation 0.73). Thirty-eight per cent of sources have straight spectra, while of the rest, over three times as many have negatively curved (downward curvature at high frequency) as positively curved spectra, which is reflected in the mean value of -0.34. For $\theta > 1$ arcsec the proportion of straight spectra and the ratio of negatively curved to positively curved spectra

is approximately the same as for all sources. The mean (−0.32) and the standard deviation (0.71) remain similar. For the $\theta \leqslant 1$ arcsec distribution, 30 per cent of spectra are straight and the ratio of negatively curved to positively curved spectra falls slightly to 2.5. The mean is −0.43, indicating a tendency for more negatively curved spectra than for the sources with $\theta > 1$ arcsec. The standard deviation is 0.83.

4.5 MORPHOLOGIES

4.5.1 Derived from brightness distributions

The morphological scheme used is described in Section 4.1. The results are summarized in Table 3(a). Fifty-three per cent of sources have FR class II morphology and only 7 per cent of sources have FR class I or class I/II morphologies. Seventeen per cent of all double sources have possible central components. Forty-one per cent of sources lack discernible structure and 12 per cent have angular sizes < 1 arcsec.

Table 3. (a) Morphologies derived from brightness distributions. Numbers in parentheses are percentages of the total.

	Class	Number	
Visible double structure	FR I	3 (5)	35 (59)
	FR I/II	1 (2)	
	FR II	31 (53)	
	With C	6 (10)	
Without double structure	E	17 (29)	24 (41)
	U	7 (12)	

Table 3. (b) Morphologies derived from spectral data. Numbers in parentheses are percentages of the total.

	U	E	U + E
(1) Compact	2 (3)	5 (8)	7 (12)
(2) Extended with C	1 (2)	5 (8)	6 (10)
(3) Extended without C	4 (7)	7 (12)	11 (19)

Table 3. (c) Summary of morphologies. Numbers in parentheses are percentages of the total.

Extended (with or without C)				
Visible double structure	FR I	3 (5)	35 (59)	52 (88)
	FR I/II	1 (2)		
	FR II	31 (53)		
Without double structure			17 (29)	
Compact				7 (12)
Extended with C				
From brightness distribution			6 (10)	12 (20)
From spectral data			6 (10)	

4.5.2 *Derived from spectral data*

For sources whose structure is poorly determined by the observed brightness distribution, it may be possible to obtain some structural information from the spectral data. Synchrotron self-absorption in regions of high brightness causes the spectrum to flatten and turn over at low frequencies. This indicates that the size of the emitting region is likely to be small ($\lesssim 10$ pc for sources with turnovers in the observable range) so that a critical brightness is exceeded. Conversely, sources with spectra that are straight or steepen at high frequency (because of synchrotron ageing in the emitting regions) are likely to have extended structure on scales much larger than this. In general, spectra may show a combination of synchrotron self-absorption and spectral ageing. High-frequency flattening would be expected for extended sources with central components, since these compact regions will eventually dominate the integrated flux density at high frequency because of their flatter spectra. At lower frequencies the relatively compact (~ 1 kpc) hotspots of some sources may show evidence of synchrotron self-absorption in their spectra, but this is unlikely to be important at these frequencies since the turnover frequency for even the smallest hotspots is not expected to exceed a few tens of MHz (unless sources in this sample differ radically from sources found in brighter samples – see also Broderick & Condon 1975).

We can thus divide sources into three categories on the basis of β and α_L (the latter is more useful than α_H because, in this simple scheme, α_L is determined only by the synchrotron self-absorption mechanism and therefore gives an unambiguous indication of the presence of compact components). The figures in parentheses given in column 14 of Table 2 for the E and U class sources refer to these spectral classifications, as follows:

(1) Compact sources, i.e. with compact regions ($\lesssim 10$ pc in size) producing more than half the total flux density at frequencies between 0.4 and 1.4 GHz: $\alpha_L < 0.5$, with negatively curved, $\beta < -\sigma(\beta)$, or straight, $|\beta| < \sigma(\beta)$, spectra.

(2) Extended sources with central components producing at least half the total flux density at frequencies between 1.4 and 2.7 or 5 GHz, but less than half between 0.4 and 1.4 GHz: positively curved $\beta > \sigma(\beta)$ spectra.

(3) Extended sources without central components: $\alpha_L > 0.5$ with negatively curved, $\beta < -\sigma(\beta)$, or straight, $|\beta| < \sigma(\beta)$ spectra.

Despite the oversimplification involved in this scheme it enables some reasonable guesses to be made as to the nature of sources classified E or U in Table 2.

The results of this classification may be summarized in a contingency table (Table 3b); the population of each portion of the table can then be determined from the data in Table 2 for the U and E sources separately. For class U there are over twice as many extended as compact sources (mostly without central components); for class E this ratio is the same (nearly half of these extended sources have central components). Taking these two classes together, 12 per cent of the sample are compact and the rest (29 per cent) are extended, while 33 per cent of these extended sources have central components.

4.5.3 *Summary of morphologies*

By combining these results (Table 3c), we find that the proportion of compact sources (or more precisely, the proportion of sources with regions of linear size $\lesssim 10$ pc which produce more than half the total flux density between 0.4 and 1.4 GHz) is 12 per cent. The rest have extended structure. Of these, 23 per cent have central components, whilst of those with visible double structure, 89 per cent have FR class II morphologies.

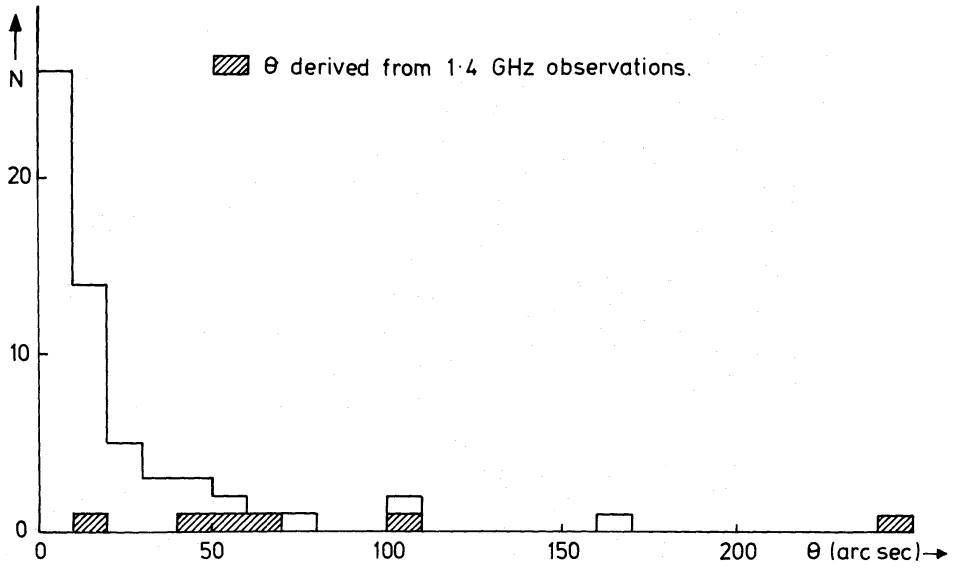

Figure 5. Distribution of largest angular size θ. Values derived from 1.4-GHz observations are shown shaded.

4.6 ANGULAR SIZE DISTRIBUTION

The distribution of the largest angular sizes is shown in Fig. 5. Hatched boxes indicate angular sizes derived from 1.4-GHz observations. The distribution shows a smooth monotonic decrease with increasing angular size, with a tail extending up to 240 arcsec. The median angular size is 12 arcsec.

5 Conclusions

These observations show that in this sample:

(1) Six sources (10 per cent) have extended structure of very low brightness, visible only at low resolution or low frequency. One of these is seen to be a highly unequal double, three have spectra typical of extended sources without compact components and two have spectra typical of extended sources with bright central components.

(2) There are two sources with projected linear sizes $\gtrsim 1$ Mpc.

(3) Two sources have very steep high-frequency spectra and very diffuse structures lacking hotspots, features which imply that the extended regions are not now being supplied with energy.

(4) Eighty-eight per cent of sources have extended structure, while the rest have compact structures. Fifty-three per cent of the total and 89 per cent of those with visible double structure have FR class II morphologies.

(5) Twenty per cent of sources have central components.

(6) Sixty-two per cent of sources have curved spectra, with over three times as many showing high-frequency steepening as show high-frequency flattening.

(7) The median angular size is 12 arcsec.

These results, together with those of the optical observations described in Paper II, will be discussed and interpreted in Paper III.

Acknowledgments

It is a pleasure to thank Ann Downes, Guy Pooley, Julia Riley and Peter Warner for expert advice and assistance, and particularly Malcolm Longair for being the prime mover. I acknowledge financial support from the SERC.

References

Baars, J. W. M., Genzel, R., Pauliny-Toth, I. I. K. & Witzel, A., 1977. *Astr. Astrophys.*, **61**, 99.

Broderick, J. J. & Condon, G. G., 1975. *Astrophys. J.*, **202**, 596.

Colla, G., Fanti, C., Fanti, R., Ficarra, A., Formiggini, E., Gandolfi, E., Gioia, I., Lari, C., Marano, B., Padrielli, L. & Tomasi, P., 1973. *Astr. Astrophys. Suppl.*, **11**, 291.

Colla, G., Fanti, C., Fanti, R., Ficarra, A., Formiggini, L., Gandolfi, E., Grueff, G., Lari, C., Padrielli, L., Roffi, G., Tomasi, P. & Vigotti, M., 1970. *Astr. Astrophys. Suppl.*, **1**, 281.

Colla, G., Fanti, C., Fanti, R., Ficarra, A., Formiggini, L., Gandolfi, E., Lari, C., Marano, B., Padrielli, L. & Tomasi, P., 1972. *Astr. Astrophys. Suppl.*, **7**, 1.

Conway, R. G., Gilbert, J. A., Kronberg, P. P. & Strom, R. G., 1972. *Mon. Not. R. astr. Soc.*, **157**, 443.

Downes, A. J. B., Longair, M. S. & Perryman, M. A. C., 1981. *Mon. Not. R. astr. Soc.*, **197**, 593.

Elsmore, B., Kenderdine, S. & Ryle, M., 1966. *Mon. Not. R. astr. Soc.*, **134**, 87.

Fanaroff, B. L. & Riley, J. M., 1974. *Mon. Not. R. astr. Soc.*, **167**, 31P.

Fanti, C., Fanti, R., Ficarra, A. & Padrielli, L., 1974. *Astr. Astrophys. Suppl.*, **18**, 147.

Folsom, G. H., Smith, A. G., Hackney, R. L., Hackney, K. R. & Leacock, R. J., 1971. *Astrophys. J.*, **169**, L131.

Galt, J. A. & Kennedy, J. E. D., 1968. *Astr. J.*, **73**, 135.

Gioia, I. M. & Gregorini, L., 1980. *Astr. Astrophys. Suppl.*, **36**, 347.

Grueff, G. & Vigotti, M., 1977. *Astr. Astrophys.*, **54**, 475.

Grueff, G. & Vigotti, M., 1979. *Astr. Astrophys. Suppl.*, **35**, 371.

Hine, R. J., 1981. *PhD thesis*, University of Cambridge.

Högbom, J. A., 1974. *Astr. Astrophys. Suppl.*, **15**, 417.

Hooley, A., Longair, M. S. & Riley, J. M., 1978. *Mon. Not. R. astr. Soc.*, **182**, 127.

Jenkins, C. J. & McEllin, M., 1977. *Mon. Not. R. astr. Soc.*, **180**, 219.

Kapahi, V. K., 1975. *Mon. Not. R. astr. Soc.*, **172**, 513.

Kapahi, V. K., 1977. In *IAU Symp. No. 74, Radio Astronomy and Cosmology*, p. 119, ed. Jauncey, D.

Kapahi, V. K., 1979. *Astr. Astrophys.*, **74**, L11.

Katgert, P., 1976. *Astr. Astrophys.*, **49**, 221.

Katgert, P., Katgert-Merkelijn, J. K., Le Poole, R. S. & van der Laan, H., 1973. *Astr. Astrophys.*, **23**, 171.

Katgert-Merkelijn, J. K., Lari, C. & Padrielli, L., 1980. *Astr. Astrophys. Suppl.*, **40**, 91.

Kraus, J. D. & Scheer, D. J., 1967. *Astrophys. J.*, **149**, L111.

Laing, R. A. & Peacock, J. A., 1980. *Mon. Not. R. astr. Soc.*, **190**, 903.

Longair, M. S., 1966. *Mon. Not. R. astr. Soc.*, **133**, 421.

Miley, G. K., 1971. *Mon. Not. R. astr. Soc.*, **152**, 477.

Neff, S. G. & Rudnick, L., 1980. *Mon. Not. R. astr. Soc.*, **192**, 531.

Olsen, E. T., 1967. *Astr. J.*, **72**, 738.

Olsen, E. T., 1970. *Astr. J.*, **75**, 764.

Peacock, J. A. & Gull, S. F., 1981. *Mon. Not. R. astr. Soc.*, **196**, 611.

Peacock, J. A. & Wall, J. V., 1981. *Mon. Not. R. astr. Soc.*, **194**, 331.

Pooley, G. G. & Henbest, S. N., 1974. *Mon. Not. R. astr. Soc.*, **169**, 477.

Rees, M. J. & Setti, G., 1968. *Nature*, **219**, 127.

Rowan-Robinson, M., 1970. *Mon. Not. R. astr. Soc.*, **150**, 389.

Ryle, M., 1962. *Nature*, **194**, 517.

Ryle, M., 1972. *Nature*, **239**, 435.

Ryle, M. & Elsmore, B., 1973. *Mon. Not. R. astr. Soc.*, **164**, 223.

Sargent, W. L. W., 1973. *Astrophys. J.*, **182**, L13.

Scheuer, P. A. G., 1977. In *IAU Symp. No. 74, Radio Astronomy and Cosmology*, p. 343, ed. Jauncey, D.

Schmidt, M., 1974. *Astrophys. J.*, **193**, 505.

Schmidt, M., 1976. *Astrophys. J.*, **209**, L55.

Stannard, D. & Neal, D. S., 1977. *Mon. Not. R. astr. Soc.*, **179**, 719.

Swarup, G. & Subrahmanya, C. R., 1977. In *IAU Symp. No. 74, Radio Astronomy and Cosmology*, p. 125, ed. Jauncy, D.

Ulrich, M.-H., Kinman, T. D., Lynds, C. R., Rieke, G. H. & Ekers, R. D., 1975. *Astrophys. J.*, **198**, 261.

Véron, M. P. & Véron, P., 1979. *Astr. Astrophys. Suppl.*, **36**, 331.

Wall, J. V., Pearson, T. J. & Longair, M. S., 1981. *Mon. Not. R. astr. Soc.*, **193**, 683.

Weiler, K. W. & Johnston, K. J., 1980. *Mon. Not. R. astr. Soc.*, **190**, 269.

Wilkinson, A., Hine, R. G. & Sargent, W. L. W., 1981. *Mon. Not. R. astr. Soc.*, **196**, 669.

Wills, D., 1979. *Astrophys. J. Suppl.*, **39**, 291.